Annals of Nuclear Energy 48 (2012) 68–83

Contents lists available at SciVerse ScienceDirect

Annals of Nuclear Energy

journal homepage: www.elsevier.com/locate/anucene

Simulated transient dynamics and heat transfer characteristics of the water boiler nuclear reactor – SUPO – with cooling coil heat extraction

A.G. Buchan [a,*], C.C. Pain [a], A.J.H. Goddard [a], M.D. Eaton [a], J.L.M.A. Gomes [a], G.J. Gorman [a], C.M. Cooling [a], B.S. Tollit [a], E.T. Nygaard [b], D.E. Glenn [b], P.L. Angelo [c]

[a] Applied Modelling & Computational Group, Department of Earth Science and Engineering, Imperial College London, London, United Kingdom
[b] Babcock and Wilcox Technical Services Group (B&W TSG), 800 Main Street, Lynchburg, VA 24504, USA
[c] NNSA Y-12 National Security Complex, Oak Ridge, TN 37831, USA

ARTICLE INFO

Article history:
Received 25 October 2011
Received in revised form 21 March 2012
Accepted 23 March 2012
Available online 15 July 2012

Keywords:
Aqueous homogeneous reactor
Fluid radiation simulation
Reactor simulation
Reactor coolant modelling

ABSTRACT

The term "water boiler" reactor refers to a type of aqueous homogeneous reactor (AHR) that was designed, built and operated by Los Alamos in the 1940s. This was the first type of liquid fuelled reactor and the first to be fuelled with enriched Uranium. For security reasons the term "water boiler" was adopted and three versions were built: LOPO (for low power), HYPO (for high power) and SUPO (for super power) which were spherical shaped reactor vessels. The name was appropriate as the reactors appeared to boil although this was actually due to the release of radiolytic gas bubbles; although SUPO was operated during some studies close to the boiling point of uranyl nitrate. The final water boiler "SUPO" was operated almost daily as a neutron source from 1951 until its deactivation in 1974-23 years of safe, reliable operation. Many of the key neutron measurements needed in the design of the early atomic weapons were made using LOPO, HYPO and SUPO. More recently SUPO has been considered as a benchmark for quasi-steady-state operation of AHRs with internal cooling structures.

This paper presents modelling and analysis of the coupled neutronic and fluid time dependent characteristics of the SUPO reactor. In particular the quasi-steady-state dynamics of SUPO have been investigated together with its heat transfer characteristics. In the simulations presented the SUPO reactor is modelled using the spatially dependent neutron/multiphase CFD simulation tool, FETCH, at a quasi-steady-state power of 25 kW. SUPO also possessed a cooling coil system that fed cooling water through the reactor for the extraction of the fission and decay heat. This cooling system, and the heat extraction, is modelled in the simulations using a new sub-modelling approach that is detailed here. The results from this simulation, such as gas fraction, gas generation rate, coolant rate and average temperature, are compared against the available experimental information.

1. Introduction

The development of the water boiler reactor at Los Alamos (Bunker, 1963; King, 1956, 1990; Los Alamos Scientific Laboratory, 1951; Bunker, 1983; Rosenthal, 2003; King, 1952; Beck et al., 1952; Lyon, 1953; Thomas, 1953; Kasten, 1954; Shorthall et al., 1954; North American Aviation, 1954; Durham, 1955; Nelson and Mann, 1955; Lane et al., 1958; Gamble, 1959; Stitt, 1959; Flora et al., 1962; Dunenfeld, 1962; Spiegler et al., 1962; Schulberg, 1965; IAEA, 2008), was made possible by the first availability of enriched uranium from Oak Ridge, and this acted as a supporting demonstration to the weapons programme on building and modelling critical assemblies. Modelling had suggested that, with a suitable reflector, criticality could be achieved with a fuel in the form of a uranyl sulphate solution when contained within a spherical stainless steel tank of diameter approximately 30 cm. It was decided to construct three reactors over 5 years. The first was a low power uranyl sulphate LOPO reactor and this was followed by the high powered (HIPO) and super powered (SUPO) reactors which contained a uranyl nitrate fuel. The SUPO design was developed in 1951 (Bunker, 1983; Rosenthal, 2003) and operated with a fuel that was enriched to 88% and was surrounded by an all graphite reflector. The highly enriched fuel meant that the reactor could reduce the amount of nitric acid decomposition whilst enhancing its reactivity. The reactor was safely operated for 23 years before being decommissioned, and was regularly run at a powers of 25 kW or more for durations that lasted several hours at a time. The success of these early water boilers resulted in the reactor technology spreading throughout the US and around the world to countries including Denmark, Japan, Germany and Italy.

* Corresponding author. Tel.: +44 020 759 49986.
E-mail address: andrew.buchan@imperial.ac.uk (A.G. Buchan).

0306-4549/$ - see front matter © 2012 Elsevier Ltd. All rights reserved.
http://dx.doi.org/10.1016/j.anucene.2012.03.027

Pictures of the SUPO reactor taken at the time of its construction are presented in Figs. 1 and 2. These show the reactor core vessel to have a spherical geometry and the coils within its body are for the feeding of cooling water for the extraction of fission and decay heat. Three separate sets of cooling coils were used which allowed higher operating powers to be studied. The SUPO's main reactivity control was achieved through two boron control rods moving within vertically aligned guide tubes – see Fig. 1 (bottom). The vessel also possessed a 'glory hole' (clearly shown in Fig. 2) that passed through its near central region and which was used for the production of neutron beams.

The SUPO reactor's design and composition has a number of interesting aspects when one considers the various physical processes that determine its behaviour and ability to operate over periods lasting several hours. Most notable would be the combination of the neutronic and fluid properties together with the various influences they have on each other. In particular, radiolytic gases that are produced by fission affect both the neutronic population and fluid dynamic flow patterns. That is, bubbles that form within the fuel solution increase voidage, thus lowering reactivity, whilst their migration to the solution surface impose drag forces that influence the fluid flow. Other properties that couple the neutron-fluid physics include the migration of the delayed neutron precursors that flow within the fluid, fission heat sources that affect fluid density and flow, and variations in the nuclear cross-sections with respect to fluid density and temperature. These processes are further affected by the SUPO geometry and internal cooling coil and guide tube structures. The presence of these will clearly affect the flow of the fluid due to drag, but also the heat exchanges with the cooling coils will further affect the solution (and neutron) dynamics. The SUPO reactor therefore provides a unique benchmark for modelling solution reactors and other AHRs, particularly with imbedded cooling coil systems. It is therefore also

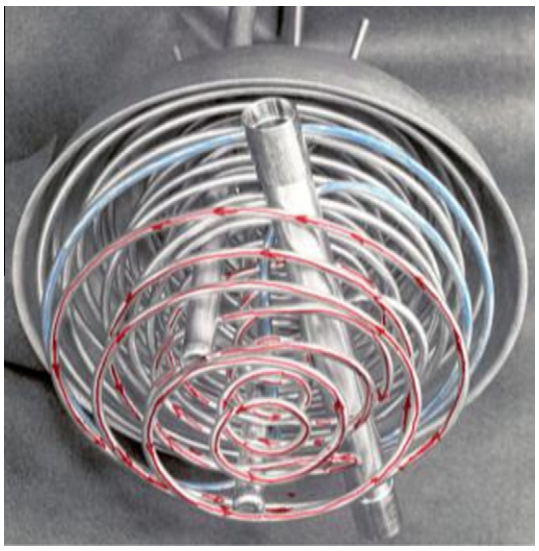

Fig. 2. View of vessel's internal parts including the inner (traced in red) and outer (traced in blue) cooling coils, glory hole and control rod guide tubes (Bunker, 1963; King, 1990). (For interpretation of the references to colour in this figure legend, the reader is referred to the web version of this article.)

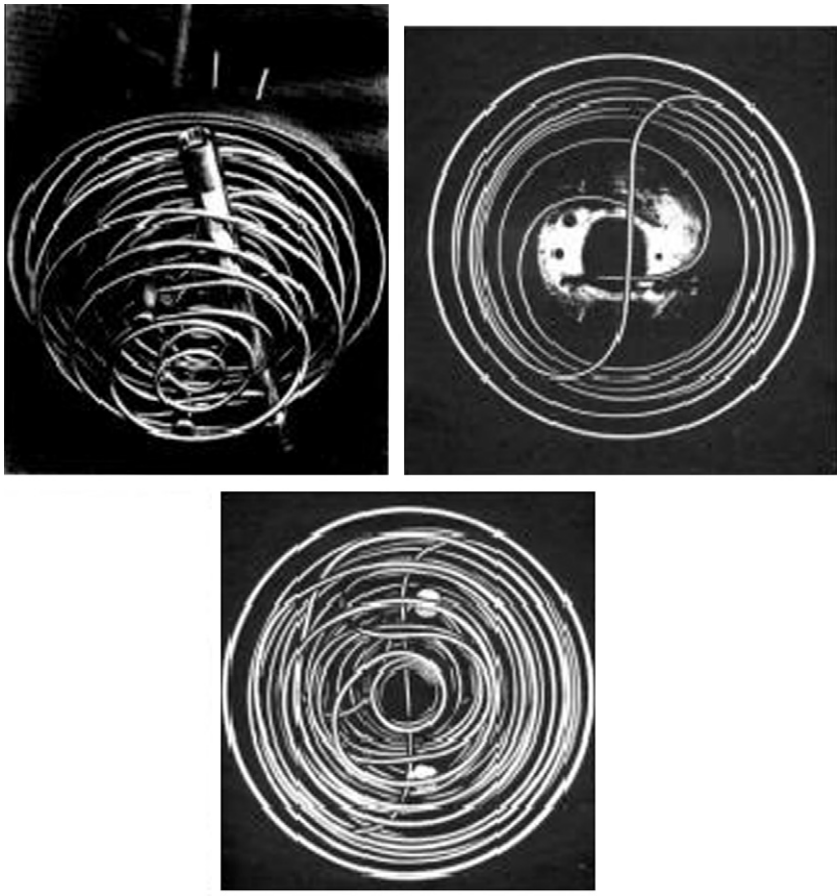

Fig. 1. Cooling coils viewed from below the upper vessel hemisphere. Above left: all three cooling tubes in place plus location of CR guide tubes and glory hole (Bunker, 1963, King, 1990). Above right: the outer cooling coil (King, 1990). Bottom: all tubes seen from axis with CR guide tubes present (King, 1990).

an ideal system for model verification for determining the various physical properties of reactors containing uranyl nitrate fuels. Key parameters such as the rates of radiolytic gas production and heat production/extraction as well as knowledge of the fissile fluid flows all play vital roles in the safe and efficient operation of such reactor types. The importance to be able to accurately model such multi-physics phenomena is therefore clear to be seen.

This article presents a study on the time-dependent and quasi-steady-state behaviour of the neutron-fluid dynamics of the SUPO reactor by its simulation using the FETCH model Pain et al. (2001a). FETCH is a multi-physics code that solves time-dependent, coupled neutron transport and fluid dynamic problems for nuclear systems, and this includes those involving fissile solutions. The temporal and spatial dependence of the neutron field is resolved using the EVENT module, de Oliveira (1986), which is based on the second order even-parity formulation of the Boltzmann transport equation. The fluid dynamics is resolved in the context of multi-phase phenomena and this is through the module FLUIDITY Pain et al. (2001b). FETCH provides the interface between these two modules. It couples them by resolving the various dependencies the two physical fields have on each other, and this is shown in Fig. 3. This illustrates the heat sources, fission distribution and delayed neutron precursors, that are created within the neutronics component through fission, being fed into the fluid calculation. In return, the spatial distribution of the delayed neutron precursor, material temperature, density and void fractions (radiolytic gas to liquid volume ratios) are fed back to the neutronics calculation. These feedback effects enable the detailed modelling of fissile solutions such that, for example, the production, transport and decay of the delayed neutron precursors can be tracked whilst they flow within the fluid. In addition, fission rates are used to calculate both dissolved radiolytic gas production and bubble formation. These bubbles are represented within the multi-phase context through a gas phase that is modelled together with the liquid phase of the fuel. This enables the bubbles' migration towards to the solution's surface to be included in the simulation and so their appearance and disappearance will be reflected in the power profile. The full coupling of these components in FETCH has helped understand the dynamics of the SUPO reactor and provide power traces that fluctuate subject to all these variables. These aspects can only be fully understood, and therefore modelled, by considering both the neutronics and fluid properties.

In the FETCH model, both the EVENT and FLUIDITY components apply finite elements in resolving the spatial dependence of their respective fields. They can resolve geometries represented in both 3D Cartesian coordinates and 2D axisymmetric (RZ) domains. The details of the two models are briefly reviewed here, and this includes a description of the equations describing radiolytic gas bubble production, transport of delayed neutron precursors, fission heat transfer onto the fluids and macroscopic cross-section generation (which vary with respect to changes in fluid density, due to gas production, and temperature). The FETCH model also allows for the movement of the control rod during a simulation and includes an algorithm that adjusts its height in order to achieve and maintain a desired power. In addition to this, in order to simulate the heat loss from the fissile solution to the cooling coil system, a new sub-model has been developed. This uses separate 1D models to represent each of the cooling coil pipes and these exchange heat with the main model's fissile solution and advects this through the pipe system. The processes of heat exchanges between the fissile solution and pipe model are described in full and comparisons of the modelled outlet temperature are made against SUPO data. The simulation of the SUPO reactor is based on it in operation at 25 kW of power which will achieve a temperature of approximately 60 °C. The control rod positions are adjusted in the model so that they respond to changes in the system's reactivity and so maintain this intended operating power. The influence of the speed of the control rod's movement on the reactor's behaviour is studied. This is accompanied by the predicted power levels, solution pressures and velocities, as well as the outflow temperatures of the cooling coil water. The results from these simulations are compared against the available experimental information (Bunker, 1963, King, 1956, 1990).

The following sections are set out as follows. Section 2 describes the SUPO design and fuel specifications with the reactor operating at its intended 25kW power level. This includes the description of the FETCH model that recasts the reactor geometry in RZ dimensions. The radiation and multi-phase flow equations solved by the FETCH model are then described in Section 3, and this includes a description of the coupling between the physical fields. The

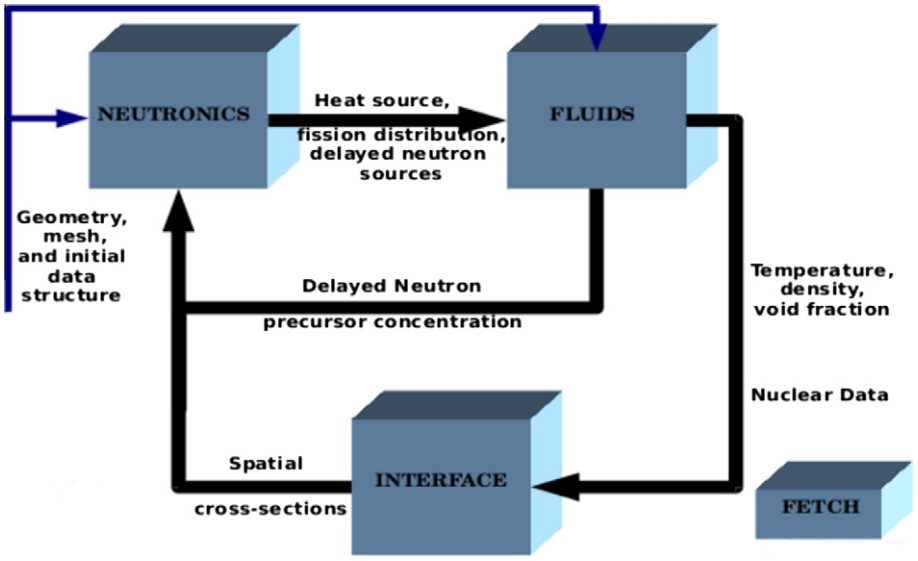

Fig. 3. This flow diagram illustrates the neutronic and fluid coupling that is performed by the FETCH model. The heat and delayed neutron precursor sources that are generated by the neutronic component are supplied to the fluids. The fluid component, in turn, return the delayed neutron precursor distribution. In addition, the temperature and density of the fluids are fed through an interface. This calculates the new nuclear cross-section data sets which are then fed back into the neutronics calculation.

description of the cooling coil sub-model, that models the heat extraction system, has been presented in its own section – Section 4. Section 5 presents the results of the FETCH simulations and the conclusion are presented in Section 6.

2. The SUPO design and specifications

The SUPO reactor design and means of operation drew heavily on experience with LOPO and HYPO. The reactor vessel described in Section 1 was enclosed and centred within a graphite reflector which was in turn extended in the form of two graphite thermal columns. This is illustrated in Fig. 4 which shows a cut-away drawing of the complete SUPO reactor. This graphite was represented, in simplified geometry, in the EVENT neutronics component of the coupled FETCH calculations. Concrete shielding enclosed the reflector and thermal columns. In addition to solution height measuring devices within the vessel there were recombiner provisions (seen mounted above the vessel in Fig. 4) to capture fission gases and gaseous products of radiolytic decomposition and also to return to the vessel aqueous condensate. The provision of guide tubes for two in-vessel boron control rods has been referred to; the boron was enriched in boron-10. In addition, two cadmium metal strip rods, very likely used as safety rods, moved in vertical aluminium frames within the graphite and tangential to the vessel outer surface. The drives for the boron rods and the aluminium frames for the cadmium rods may be seen in Fig. 4. In her report, Bunker (1963) describes the 25 kW reference case and also gives control rod worth data. In addition to the glory hole, a second tube tangential to the vessel exterior may be seen. In order to reduce peak solution temperatures within the vessel, presumably to reduce the margin before boiling, the inlet water to all three cooling tubes was reduced to 5 °C using a chiller. Bunker also discusses the detailed heat balance in SUPO under operating conditions: as a proportion of total fission power she ascribes ~2% and ~6%, respectively, to heat removed by the condenser and to heat lost by the vessel through conduction into the graphite reflector. The present authors expect to perform modelling to investigate these factors in future work. The factors given by Bunker are broadly consistent with data given by Durham (1955).

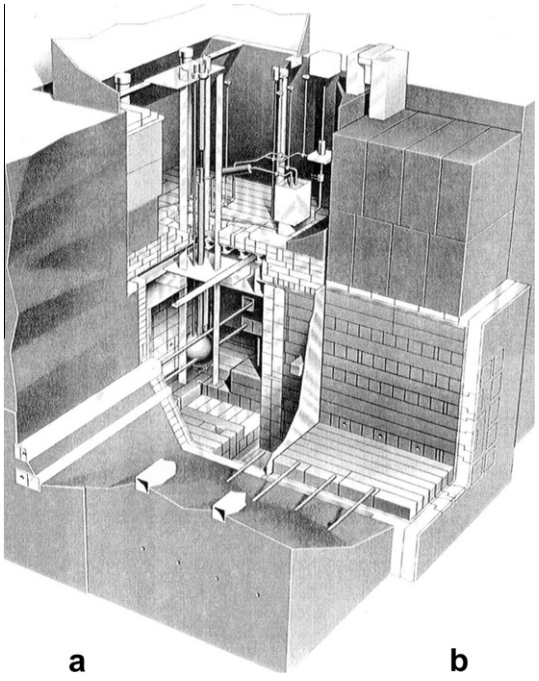

Fig. 4. Cutaway drawing of SUPO (Bunker, 1963; King, 1990)

As described by Bunker, the SUPO reactor has a spherical shell made from two welded hemispheres constructed from stainless steel with thickness 0.15 cm and outer dimension 30.48 cm. It contains a soup of uranyl nitrate that occupies a volume of 12,572 cm^3 (at 60 °C) with Table 1 listing a breakdown of its constituent isotopes. The three cooling coils have identical submerged length of 20 ft, they have inner and outer diameters 0.476 cm and 0.635 cm respectively, and displace the fluids by a total volume of 550 cm^3. The control rod guide thimbles enter the solution to a depth of approximately 23 cm, with each displacing the fluids by 64.9 cm^3. The glory hole is a stainless steel tube of diameter 2.8 cm, and enters the vessel by a length of 27.28 cm which displaces the fluids by 240 cm^3. These specifications are considered the basic data set describing the conditions of the reactor.

2.1. The RZ semi-explicit model of the SUPO reactor

The FETCH model used in the SUPO simulation has made use of the reactor's spherical geometric features and has been represented in 2D RZ geometry. This was chosen as it allows the use of a fine spatial resolution mesh that can resolve much of the dynamics around the cooling coils whilst keeping CPU run time relatively low. The cooling coils within the FETCH model are explicitly resolved, and as a result much of the physics behind SUPO flow dynamics can be determined. Although the 3D dynamics of SUPO may be different in detail from the RZ dynamics, the 2D approach can (in the absence of a parallel highly resolved 3D FETCH model) yield results distinct from those from a 3D model. This is because a 3D simulation will require a more parameterised model when running in a serial environment.

The key geometric features of SUPO requires an unstructured finite element mesh to accurately represent the solution geometry as well as the surrounding steel vessel and graphite (see Fig. 5). Each intersection of the cooling coil with the RZ-geometry is explicitly resolved. The volume of each intersection is maintained so that it is the same as the cooling coil pipes cross sections. To simplify the explicit meshing of cooling coils pipes, their geometry was made rectangular with the same equivalent cross sectional area. The model mimics the idealised geometry of the pre-construction engineering drawings, and the distribution of cooling coils are represented as sets of nesting helices. The three coils are represented by six separate sets of vertically aligned circular rings of tubing. Each tube is 609.6 cm (20 ft) in length and makes up an appropriate pair (the cooling water flows down one coil and up another), together with the necessary length of pipe to connect with the vessel head. The dimensions of the cooling coils are listed in Table 2. Due to the dominance of the circumferential component of the tube length for a helix, only for the first inner set of tube rings is it necessary to correct for the non-horizontal alignment of the original helical structures. That is, the helices are slightly adjusted to ensure the correct quantity of mass is submerged within the solution. Finally, although the glory hole is completely ignored in this geometry, the control rod has been represented but its presence is only made to be felt by the neutrons. The control rod guide tube can be seen to enter the reactor's vessel through its top right section, and the control rod can move vertically within this sleeve to adjust reactivity. However the sleeve itself is arranged so as not to affect the solution flow patterns. This

Table 1
Approximate gram weights of soup constituents that forms a solution with total a volume of 12,700 cm^3.

Isotope	U235	U238	N	H	O
Weight (g)	950	120	190	1410	11,960

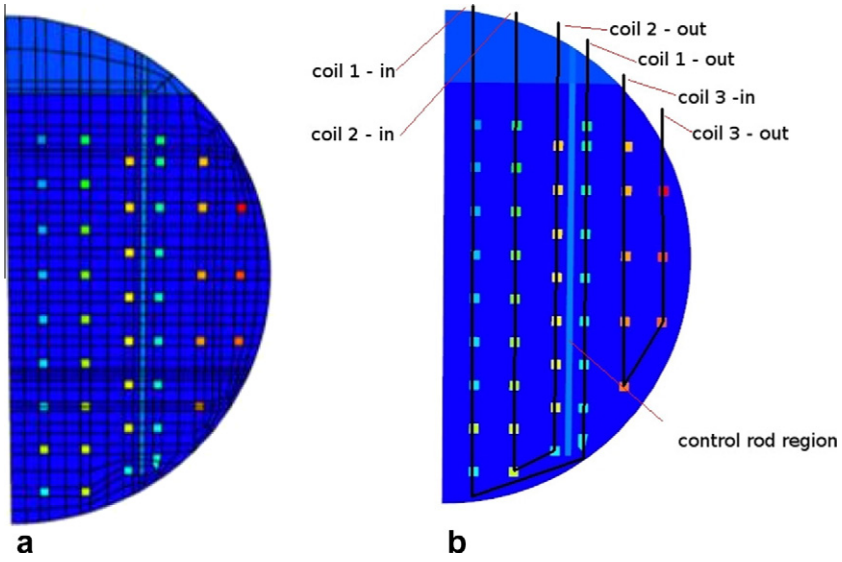

Fig. 5. (a) Geometry of SUPO's fuel section including the mesh and the intersection of the cooling coils with the RZ domain. There are 849 quadrilateral finite elements and 899 nodes and this is the domain used for the fluids part of the FETCH calculation. A finer mesh is produced by splitting each element into four and thus there are 4×1267 elements in the fine mesh simulation. (b) The sequence and direction of flow of the cooling water within the three sets of cooling coils are outlined by the black lines. The region occupied by the control rod is also indicated – although its presence will only be felt by the neutronic field.

Table 2
Dimensions and flow directions of the cooling coil helices used in SUPO model.

Ring number	(Pipe) and flow direction	Radius (cm)	Circumference (cm)	Separate rings	Tube length (cm)
1	(1) down	1.95	12.25	9	110.3
2	(2) down	4.40	27.65	9	248.8
3	(2) up	6.94	43.60	8	348.9
4	(1) up	8.65	54.35	9	489.4
5	(3) down	11.12	69.87	5	349.4
6	(3) up	13.35	83.88	3	251.6

is because its representation and location in the RZ geometry will create a solid barrier between the inner and outer regions of the reactor's upper hemisphere. Instead, the fluid can flow through the control rod section as though it was not there.

The mesh in the SUPO reactor has been designed not to contain a large number of finite elements so that the FETCH simulations can run rapidly. A FETCH simulation of SUPO takes about 2 h to perform approximately 30 min of real time. It takes about 10 min of simulation time for the SUPO system to reach a quasi-steady-state where, in a time-averaged sense, the heat losses (to the cooling coil water) are balanced by the fission heat source and the control rod algorithm is maintaining a quasi-steady-state condition.

3. The FETCH model for SUPO

This section provides a brief outline of the FETCH model and states the equations that are solved for modelling the transport of neutrons and the solution's fluid dynamics. In modelling the SUPO reactor the solution is resolved in the context of multi-phase flow where it is considered as a mixture of both liquid and gas phases. The latter of these phases is used to account for the production of radiolytic gas bubbles within the simulation. This section also includes a description of the coupling between the radiation and fluid fields and describes how fluid heat sources are generated, how dissolved gas and bubbles are produced and how these feed back into the nuclear material cross-section data.

3.1. Neutron transport module: EVENT

EVENT is a general purpose radiation transport model used in radiation shielding, reactor and criticality calculations in both transient and non transient modelling. Its formulation is based on a second order even-parity principal, which can be formed from the first order Boltzmann transport equation that describes the transport of neutral particle radiation,

$$\frac{1}{v}\frac{\partial}{\partial t}\psi(\mathbf{r},\mathbf{\Omega},E,t)+\Omega\cdot\nabla\psi(\mathbf{r},\mathbf{\Omega},E,t)+\mathcal{H}\psi(\mathbf{r},\mathbf{\Omega},E,t) = \mathcal{S}(\mathbf{r},\mathbf{\Omega},E,t). \quad (1)$$

The variable $\psi(\mathbf{r},\mathbf{\Omega},E,t)$ denotes the particle intensity (or angular flux) in the 7 dimensional phase-space of space ($\mathbf{r}$), angle ($\mathbf{\Omega}$), Energy (E) and time (t). The particle velocity is denoted by v. The first term of the equation describes the rate of change in the particle distribution (w.r.t. time) through a small volume in phase-space. This accounts for particles streaming out of the volume (the second term) as well as those being absorbed and scattered by the material (the third term). This scattering and removal operator is expressed fully as:

$$\mathcal{H}\psi(\mathbf{r},\mathbf{\Omega},E,t)\equiv\sigma_t(\mathbf{r},E,t)\psi(\mathbf{r},\mathbf{\Omega},E,t)-\int_{4\pi}dE'\int_{4\pi}d\mathbf{\Omega}'\sigma_s(\mathbf{r};\mathbf{\Omega}' \rightarrow \mathbf{\Omega},E'\rightarrow E,t)\psi(\mathbf{r},\mathbf{\Omega}',E',t). \quad (2)$$

where σ_t and σ_s denote the macroscopic cross-sections. The term on the right of Eq. (1) accounts for any source of particles which may originate from external sources ($\mathcal{S}_{ext}$), through fission events or from the decay of delayed precursors:

$$\mathcal{S}(\mathbf{r},\mathbf{\Omega},E,t)\equiv\mathcal{S}_{ext}(\mathbf{r},\mathbf{\Omega},E,t)+\frac{(1-\beta)}{4\pi}\chi_p(E)\int d\mathbf{\Omega}'\times\int_{4\pi}dE'\nu\sigma_f(\mathbf{r},E',t)\phi(\mathbf{r},\mathbf{\Omega}',E't,)+\sum_k\lambda_k\chi_k^d(E)\,D_k. \quad (3)$$

The term $D_k(r,t)$ denotes the precursor concentration for delayed group k and $\nu\sigma_f$ is the average number of neutrons emitted per fission, multiplied by the fission cross-section. β is the sum of delayed precursor fractions which, in this article, is comprised

from 6 precursor groups that have half lives λ_k. The terms $\chi_p(E)$ and $\chi_k^d(E)$ denote the spectrum of the prompt fission neutrons and delayed fission neutrons (from precursor group k) respectively.

By applying a time discretisation such backward Euler to the time term of Eq. (1), one can fold the temporal information within the scatter/removal and source terms to form the following expression of the flux at the end of a time step:

$$\Omega\cdot\nabla\psi(\mathbf{r},\mathbf{\Omega},E,t)+\mathcal{H}^*\psi(\mathbf{r},\mathbf{\Omega},E,t)=\mathcal{S}^*(\mathbf{r},\mathbf{\Omega},E,t). \tag{4}$$

The terms introduced here are defined as $\mathcal{H}^*=\mathcal{H}+\frac{1}{v\Delta t}$ and $\mathcal{S}^*=\mathcal{S}+\frac{\psi_0}{v\Delta t}$ with ψ_0 denoting the flux at the beginning of the time step. This enables one to solve a sequence of time independent equations where the flux at each time step is found using its solution from the previous step as a component of its source. Now using a multi-group approach for treating the energy dependence, a mono energetic time independent transport equation can be considered (i.e. E is now dropped). The solution procedure is to then form the even and odd parity variables of the angular flux (ψ^+ and ψ^- respectively):

$$\psi^+=[\psi(\mathbf{\Omega})+\psi(-\mathbf{\Omega})]/2 \text{ and } \psi^-=[\psi(\mathbf{\Omega})-\psi(-\mathbf{\Omega})]/2, \tag{5}$$

together with similar parity variables of the source term,

$$\mathcal{S}^{\pm}=[\mathcal{S}(\mathbf{\Omega})\pm\mathcal{S}(-\mathbf{\Omega})]/2. \tag{6}$$

Eq. (4) is then expressed in terms of $-\mathbf{\Omega}$:

$$-\Omega\cdot\nabla\psi(\mathbf{r},-\mathbf{\Omega},t)+\mathcal{H}^*\psi(\mathbf{r},-\mathbf{\Omega},t)=\mathcal{S}^*(\mathbf{r},-\mathbf{\Omega},t), \tag{7}$$

which is then added and subtracted from Eq. (4). By substituting in the expressions (5) and (6), the following two sets of equations are formed:

$$C\psi^+=\mathcal{S}^+-\mathbf{\Omega}\cdot\nabla\psi^-, \tag{8}$$

$$G^{-1}\psi^-=\mathcal{S}^--\mathbf{\Omega}\cdot\nabla\psi^+. \tag{9}$$

The two operators C and G define the removal terms minus the even and odd components of the distributed scattering $\mathcal{H}$ operator, respectively.

$$C\psi(\mathbf{r},\mathbf{\Omega})=\sigma_t\psi(\mathbf{r},\mathbf{\Omega})-\int_{4\pi}d\mathbf{\Omega}'\sigma^+(\mathbf{r};\mathbf{\Omega}.\mathbf{\Omega}')\psi(\mathbf{r},\mathbf{\Omega}'), \tag{10}$$

$$G^{-1}\psi(\mathbf{r},\mathbf{\Omega})=\sigma_t\psi(\mathbf{r},\mathbf{\Omega})-\int_{4\pi}d\mathbf{\Omega}'\sigma^-(\mathbf{r};\mathbf{\Omega}.\mathbf{\Omega}')\psi(\mathbf{r},\mathbf{\Omega}'). \tag{11}$$

Eqs. (8) and (9) can now be combined to eliminate the odd parity moments and form the second order differential equation only in terms of the even parity variables.

$$-\mathbf{\Omega}\cdot\nabla\mathcal{G}\mathbf{\Omega}\cdot\nabla\psi^++\mathcal{C}\psi^+=\mathcal{S}^+-\mathbf{\Omega}\nabla\mathcal{G}\mathcal{S}^- \tag{12}$$

In obtaining the solution to this formulation, the neutron scalar flux at position $\mathbf{r}$ can be recovered through the following relationship with the even-parity function:

$$\phi(r)=\int\psi(\mathbf{r},\mathbf{\Omega})d\mathbf{\Omega}=\int\psi^+(\mathbf{r},\mathbf{\Omega})d\mathbf{\Omega}, \tag{13}$$

from which the power of the reactor at a given time instance is given as:

$$\text{Power}=w\int_v\int_E\sigma_f\phi(r,E). \tag{14}$$

where w represents the energy released per fission – w = 200 MeV. A similar relationship can be defined relating the solution's current with the odd parity variables.

$$J(r)=\int\mathbf{\Omega}\psi(\mathbf{r},\mathbf{\Omega})d\mathbf{\Omega}=\int\mathbf{\Omega}\psi^-(\mathbf{r},\mathbf{\Omega})d\mathbf{\Omega}. \tag{15}$$

The solution of Eq. (12) can be shown to be equivalent to mnimising the functional:

$$\mathcal{F}[\psi]=(\mathbf{\Omega}\nabla\psi,\mathcal{G}\mathbf{\Omega}\nabla\psi)+(\psi,\mathcal{C}\psi)-2(\psi,\mathcal{S}^+)-2(\mathbf{\Omega}\nabla\psi,\mathcal{G}\mathcal{S}^-), \tag{16}$$

which is the approach taken in the EVENT module, with full details given in Pain et al. (2001a). The discretisation methods used to resolve the dimensions of this equation are as follows. Spherical harmonics are used to discretise the angular dimensions, and in this article a P_1 resolution is used throughout. As already stated, bi-linear finite elements are used to discretise the spatial domain, Backward Euler is applied in time and multi-group in energy.

3.2. Multi-phase solver: FLUIDITY

FLUIDITY solves the multi-phase flow equations which, in the context of this article, involves the two phases of liquid and gas. For each phase three conservation equations are solved that conserve the mass, momentum and thermal energy. The mass equations are used to track the volume fraction α_k, density ρ_k and velocity v_k of each phase k and is given by the equation,

$$\frac{\partial}{\partial t}(\alpha_k\rho_k)+\nabla\cdot(\alpha_k\rho_k v_k)-\nabla\cdot\rho_k\gamma_k^c\nabla\alpha_k-S_k^m=0, \tag{17}$$

where S_k^m denotes a source of mass. In the momentum equations the momentum exchanges between the phases are conserved. However, they also account for interfacial pressure M_k^p and drag forces M_k^d, virtual mass M_k^{vm} and lift M_k^L, Soo (1990). For phase k the momentum equation is given as,

$$\begin{aligned}\frac{\partial\alpha_k\rho_k v_k}{\partial t}+\nabla\cdot\alpha_k\rho_k v_k v_k=&-\alpha_k\nabla p+\nabla\cdot\alpha_k(\tau_k)+\alpha_k\rho_k g\\&+(G_k u_k-G_{k'}v_{k'})+M_k^p+M_k^d\\&+M_k^{vm}+M_k^L,\end{aligned} \tag{18}$$

where the force terms are defined as force per unit volume, p is the shared pressure of all phases, g the gravitational acceleration and τ_k the viscous stress tensor. The viscous stress tensor is given by $\tau_k=\mu_k\frac{1}{2}[\nabla v_k+\nabla v_k^T]$ where the superscript 'T' denotes the transpose of ∇v_k and μ_k is the viscosity of phase k. The terms involving $G_k, G_{k'}$ represent the momentum exchange between the phases due to a transfer of mass (momentum) from one phase to another and visa versa. The subscript k' is attached to variables associated with phases other than those of the liquid and gas.

The equation for conserving internal energy of the liquid phase e_l is given by:

$$\begin{aligned}&\frac{\partial}{\partial t}(\alpha_l\rho_l e_l)+\nabla\cdot(\alpha_l\rho_l v_l e_l)+p(\nabla\cdot\alpha_l v_l+\nabla\cdot\alpha_g v_g)\\&\quad=\nabla\cdot\alpha_l\gamma_l^e\nabla T_l+Q_l+\Gamma_l.\end{aligned} \tag{19}$$

It is assumed that e_l is related to liquid temperature T_l by $e_l = C_{vl}T_l$, where C_{vl} denotes the specific heat capacity at constant volume. The interface exchange terms Γ_k satisfy $\sum_k\Gamma_k=0$ and γ_k^e represents molecular and turbulent diffusion. The rate of energy deposition Q_l results from fission and is discussed in the next subsection.

The gas phase's thermal energy (e_g) accounts for the radiolytic gas bubble temperature. Its equation is formed using the thermal energy equation for a bubble as given in Soo (1990). By summing over the bubbles within a fluid volume the resulting equation of the gas phase can be expressed as:

$$\alpha_g\rho_g\frac{\partial}{\partial t}(e_g)+\alpha_g\rho_g\nabla\cdot(v_g e_g)=\nabla\cdot\alpha_g\gamma_g^e\nabla T_g+\Gamma_g,$$

where a turbulent diffusion term involving γ_g^e has been introduced into this equation.

3.3. FETCH interface modules

The FETCH interface modules that link the fluid and radiation fields are described here.

3.3.1. Delayed neutron precursors

The transport of the delayed neutron precursors are modelled by FLUIDITY within the liquid phase l of the solution. The precursor concentration for delayed group j is denoted by $\alpha_l D_j(r, E, t)$ and is represented by the equation:

$$\frac{\partial \alpha_l D_j}{\partial t} = -\nabla \cdot v_l \alpha_l D_j - \lambda_j \alpha_l D_j + \beta_j \int_{4\pi} d\Omega \int_0^{\infty} dE v \sigma_f(E)\ \phi(\Omega, E),$$

in which v_l is the velocity of the liquid. The final term in this equation relates to the source of precursors and this is linked with the radiation field. It is created from a fraction of the fission events that occur within the fluid element where, as already described, this fraction is denoted by β_j. The sink term comes from the decay of the precursor (with half life λ_j), which, in turn, will act as a source in the neutron field. Note that the neutrons created from the decay of a precursor will have their own unique energy spectrum.

3.3.2. Heat transfer

The energy Q_l deposited in the fluid enters only the liquid phase of Eq. (19) and this arises from the fission events within the radiation field. The source term is therefore defined as the reactor's power given in Eq. (14):

$$Q_l(r,t) = \int dE\ w\sigma_f(r,E,t)\ \phi(r,E,t),$$

which is the total number of fissions occurring in the fluid element multiplied by the recoverable heat energy per fission w, which in this case is taken as 200 Mev.

3.3.3. Macroscopic cross-section nuclear data

The macroscopic cross-section material data used in the neutronic calculation is dependent on both the solution temperature and its gas saturation. The material's temperature dependency is resolved by the pre-generation of tables of cross-sections in WIMS9 (Newton and Hutton, 2002), which range in temperature from 20 °C to 100 °C at 10 °C intervals (where it is assumed the solution is pure liquid, i.e. $\alpha_l = 1$). The cross sections are then calculated individually for each element of the neutronic mesh. Each cross section is found by linearly interpolating across the cross-section tables at the element's solution temperature. In addition to this, the density of the fluid is then taken into account by multiplying the macroscopic cross-sections by liquid volume fraction. This takes into account the voidage introduced by the gas bubble production.

3.3.4. Radiolytic gas production

Whilst the continuity of the gas and liquid phases of the solution are represented in Eq. (17) an additional equation for the dissolved radiolytic gases is given by:

$$\frac{\partial \alpha_k C_k}{\partial t} + \nabla \cdot q_k \alpha_k C_k = \nabla \cdot \alpha_k \mu_k^c \nabla C_k + S_k^c + F_k^c, \tag{20}$$

for which the equation is solved for the scalar concentration C_l of dissolved radiolytic gas within the liquid ($k = l$). In this the interface exchange obeys $\sum_k F_k^c = 0$ (described below) and μ_k^c represents molecular and turbulent diffusion. The source for the production of radiolytic gas (from fission) that is dissolved in fissile liquid is given by:

$$S_l^c = \int dE\ \Lambda \sigma_f^l(r,E,t)\ \phi(r,E,t),$$

where $\Lambda = 10^{-17}$ represents grams of gas liberated per fission (which was found from experiment Barbry and Fouillaud (1996)). The term $\sigma_f^l \approx \alpha_l \sigma_f$ adjusts the fission cross-section so that it corresponds to the volume fraction of the liquid phase of the solution. The terms G_l, G_g introduced in Eq. (18) can now be defined as $G_l = F_l^c$ and $G_g = F_g^c$, and thus the sources of mass in the continuity Eq. (17) is given by:

$$S_l^m = (G_l - G_g), S_g^m = -(G_l - G_g).$$

The expression for the interface exchange F_l^c and F_g^c is described in more detail in Pain et al. (2001a), which correlates the rate of dissolved gas forming into bubbles in terms of Henry's law. However, in fissile solutions a number of processes contribute to the formation and destruction of bubbles which include; turbulence, coalescence and bursting when pearced by fission fragments. With so many unknowns, the modelling of bubble formation and concentration is made to match experimental observations. In this article the exchanges between dissolved gas and bubbles is given as:

$$F_l^c = X(C_l - C_0), F_g^c = -F_l^c, \tag{21}$$

where X denotes a bulk diffusion parameter (Mather et al., 1996, Mather and Barbry, 1991). By correlating with experimental data and following closely to (Mather et al., 1994, 1996, Mather and Barbry, 1991), the following expression for the diffusion parameter is given as:

$$X = h(C_l - C_0)\alpha_l \widehat{X}(C_l).$$

The value $\widehat{X}$ is correlated to match the pressure traces of experimental results using $\widehat{X}(C_l) = N(C_l - \widehat{C}_0)^n$ in which $\widehat{C}_0$ is the gas diffusion threshold at ambient temperature and zero solution pressure. That is, the pressure in the bubbles is from surface tension only when the bubble has radius $r_0 = 2 \times 10^{-2}$ cm. h denotes the heavyside function and its use prevents gas bubbles from dissolving back into the liquid. The values of N and n have been estimated from the Silene experimental data which found values $N = 4.71 \times 10^{16}$ and $n = 3$. It should be noted that the Silene experiment used a uranyl nitrate solution and so is similar to that of the SUPO's fuel.

4. Cooling coil modelling

This section presents the formulation for resolving the heat exchanges between the fissile solution and cooling coil system whilst the cooling fluid is pumped through it. With the SUPO model represented in RZ geometry it is not appropriate to model the cooling water system explicitly. Instead, a 1D sub-model approach is used to resolve the cooling water's temperature and simulate the heat flow as the cooling water advects along the length of the pipe. Heat is then exchanged between the 1D sub-model and the SUPO model by calculating the appropriate heat transfers on the regions where the pipe surfaces come into contact with the fissile solution. It was shown in the previous section that the meshing of the SUPO model had explicitly resolved the pipe regions which cut the RZ plane. The heat that exchanges between the fluids and coil will therefore only be on the elements that are adjacent to the elements occupied by the pipe. This section describes how the appropriate heat transfers takes place together with the sub-model for advecting the heat through the pipe system.

4.1. Thermal energy equations for the fissile solution and pipes

The multi-phase equation for the temperature of the fissile liquid phase T_l is given in Eq. (19). To develop the pipe submodel, it is only necessary to consider the advection component of the equation, together with the heat source and the heat exchange

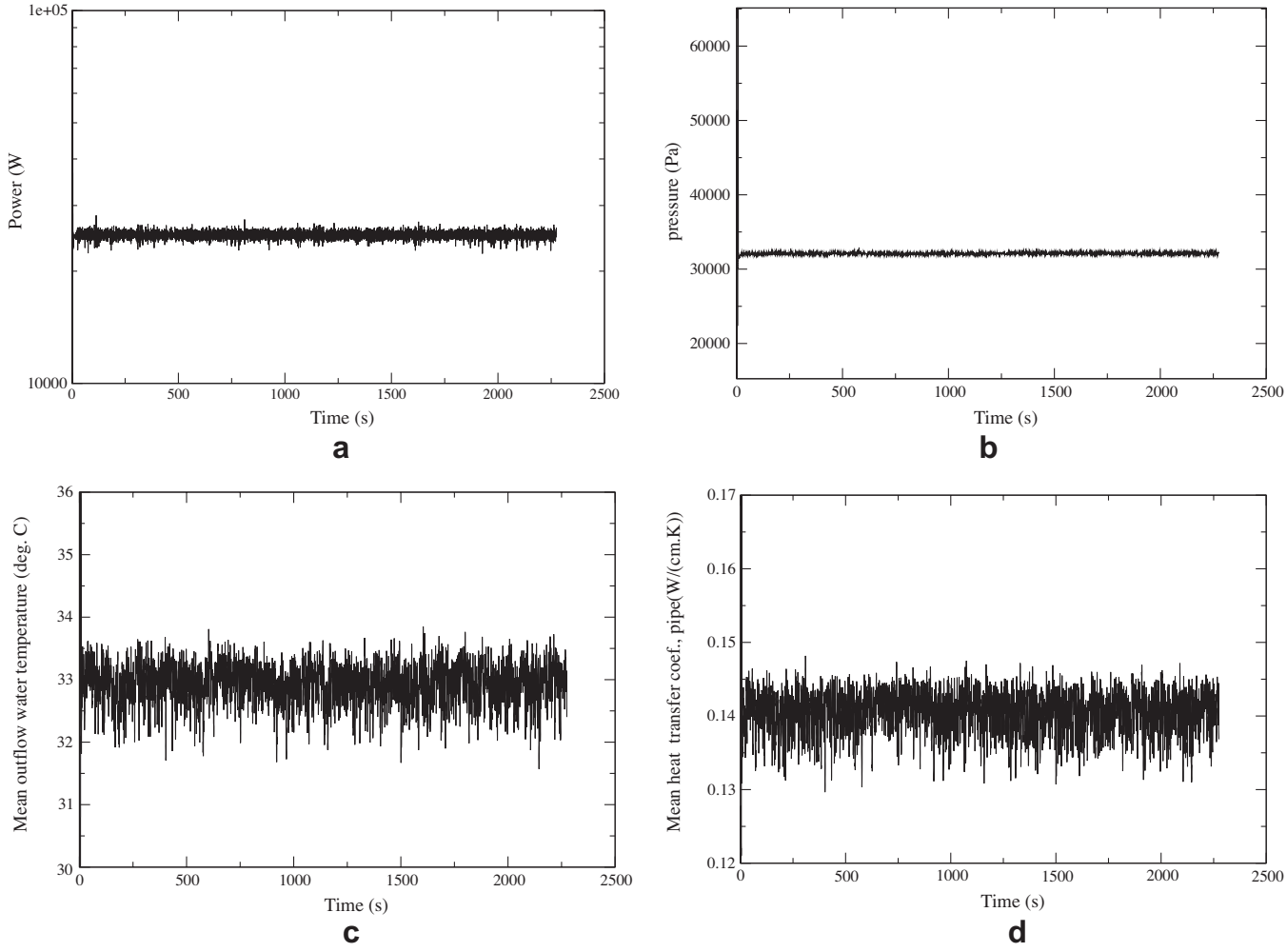

Fig. 6. Real time series of several fields: (a) power (in W), (b) maximum pressure (in g cm^{-1} s^{-2}), (c) mean outlet cooling water temperature (in °C) and (d) mean heat transfer coefficient in the cooling water fissile solution system (in W cm^{-1} K^{-1}).

terms with the pipe. The temperature equation for the liquid phase is therefore given by:

$$C_{pl}\rho_l\alpha_l\frac{D_{u_l}T_l}{Dt}+\sigma_l T_l-\sigma_l T_{coil}=S_{Tl}, \tag{22}$$

or

$$C_{pl}\rho_l\alpha_l\frac{D_{u_l}T_l}{Dt}+\sigma_l T_l=S_l, \tag{23}$$

with $S_l = S_{Tl} + \sigma_l T_{coil}$ and $\frac{D}{Dt}=\frac{\partial}{\partial t}+u\cdot\nabla$, where u is the velocity of the liquid. The terms C_{pl},ρ_l and α_l denote the fissile liquid's specific heat capacity, density and liquid fraction (the fraction is divided between the contributions of the liquid and gas phases occupying the fluid element). The terms σ_l denotes a sink term of temperature which accounts for the heat loss from the fissile solution to the cooling coil system, the coil's temperature is denoted by T_{coil}. S_{Tl} denotes the external sources of heat supplied to the fluid. This comprises of the energy generated through fission; however, in Eq. (23) the source term is also wrapped within the fluid heat sources/sinks relating to the heat exchanges with the coils.

The method of discretisation of the spatial dependence of the temperature equation is through a control volume method which uses suitable flux limiters to ensure good solution accuracy. The control volumes for the fissile solution temperature are defined as the same finite elements used to discretise the domain, and their respective function are denoted by M_e, $e\in\{1,2,\ldots,N_{ele}\}$, where N_{ele} denotes the number of control volumes or elements. These control volume functions are of the value 1 within their control volume and 0 outside, thus the resulting temperature profile will be piece-wise constant over the control volumes. This approximation is given by:

$$T_l=\sum_e M_e T_{le}. \tag{24}$$

The heat equation that is solved for each pipe in the model is given by:

$$V_R C_{p_{st}}\rho_{st}\frac{\partial T_{st}}{\partial t}+C_{p_w}\rho_w\frac{D_{u_w}T_w}{Dt}+\sigma_w T_w-\overline{\sigma_w T_l}=0, \tag{25}$$

or alternatively,

$$V_R C_{p_{st}}\rho_{st}\frac{\partial T_w}{\partial t}+C_{p_w}\rho_w\frac{D_{u_w}T_w}{Dt}+\sigma_w T_w=S_w, \tag{26}$$

where $S_w=\overline{\sigma_w T_l}$ (the over line indicates that the heat source comes from the main FETCH model and this will be averaged in some sense as described below). These equations resolve the temperature of the coil's water T_w and steel T_{st} components. The terms C_p and ρ denote the steel and water specific heat capacity and density, respectively, and V_R denotes the volume ratio of the pipe's steel and cooling water. Similar to the previous equation, the term σ_w denotes the

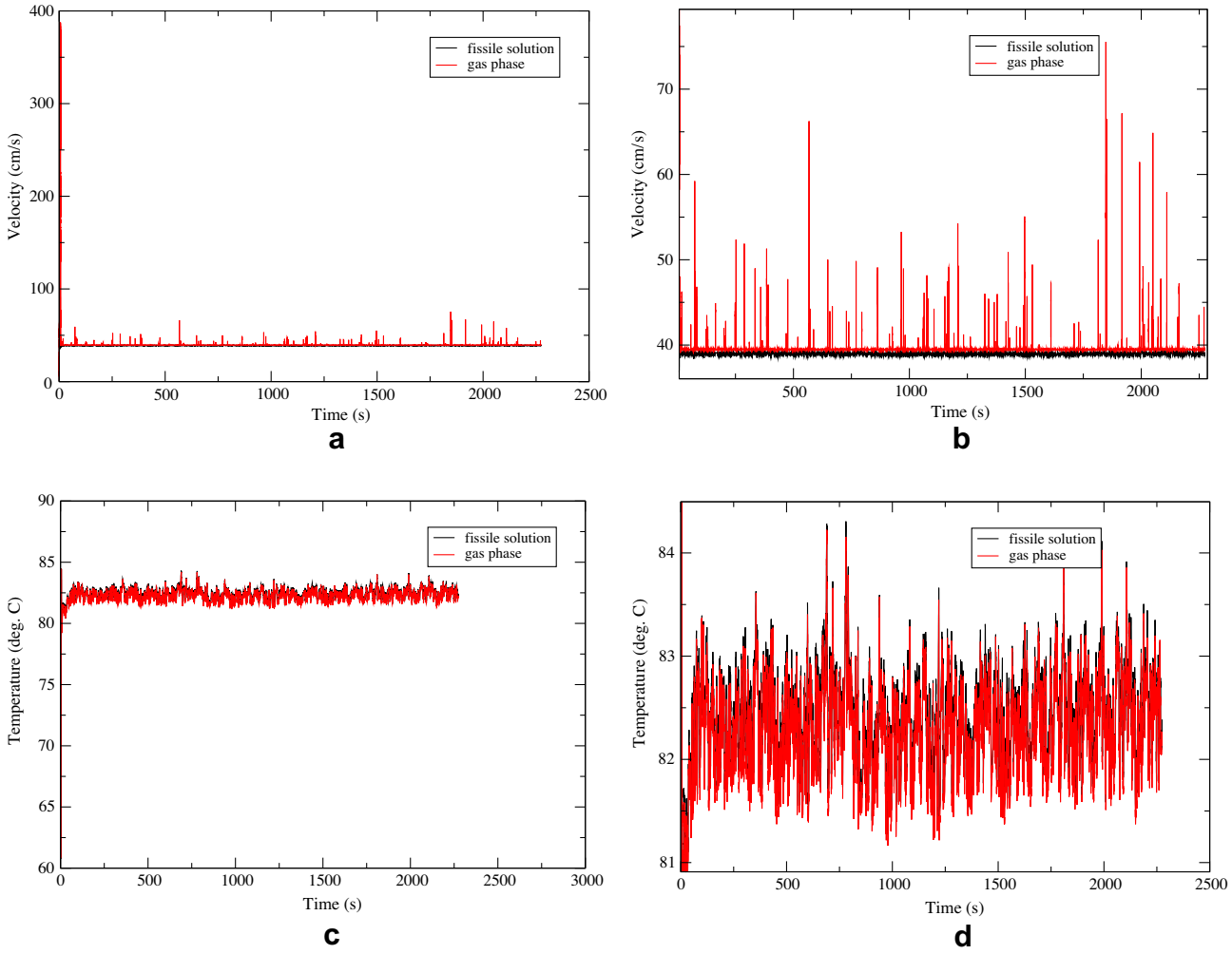

Fig. 7. The real time series simulation of: (a and b) the maximum gas and liquid velocities; (c and d) the maximum gas and liquid temperatures.

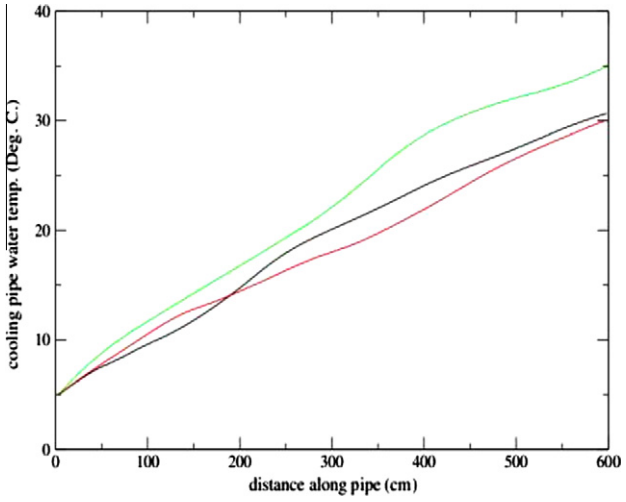

Fig. 8. The graph show the temperature distribution of the cooling water along the three pipes whilst SUPO is operating at a quasi-steady-state 25 kW power. The lines coloured black, red and green represent the distributions of the first, second and third cooling coil sets respectively. (For interpretation of the references to colour in this figure legend, the reader is referred to the web version of this article.)

sink (or in this case source with $T_l > T_w$) terms that represents the heat exchanging from the fissile solution to the pipe. These source and sink terms for exchanging heat are described in more detail below.

In resolving the time dependence of Eq. (26) sub-cycling is used with time step sizes $\Delta t_{pipe} = min\left\{\Delta t, 0.1\frac{\Delta x_{pipe}}{U_{pipe}}\right\}$. A high-resolution control volume finite element method is applied to discretise the heat equation in space. In this approach the spatial domain is divided into a finite number of non-overlapping elements over which the heat varies with a piece-wise constant variation. That is, the temperature of the pipe water is represented as:

$$T_w = \sum_e Q_e T_{we}, \tag{27}$$

where Q_e are the control volume basis functions (which have the value 1 inside their element and 0 elsewhere) and $T_{w\,e}$ their corresponding expansion coefficients.

4.2. Calculating the heat transfer coefficient

The transfer of heat from the fissile solution to the pipe is correlated from the Nusselt number:

$$Nu = a_1 + a_2(Re_{pipe}Pr_{fluid})^{\frac{4}{5}}, \tag{28}$$

for which the values used are $a_1 = 5$ and $a_2 = 0.025$. Using SGI units (cm and g) the values of the Prandtl number is given as $Pr_{fluid} = 2.842$, the kinematic viscosity of the fissile solution is given by

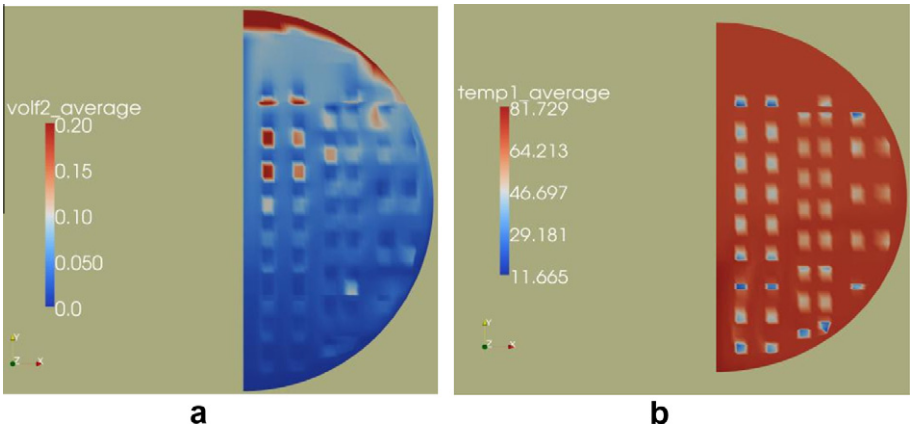

Fig. 9. Time-averaged of: (a) gas volume fraction and (b) fissile solution temperature (in °C).

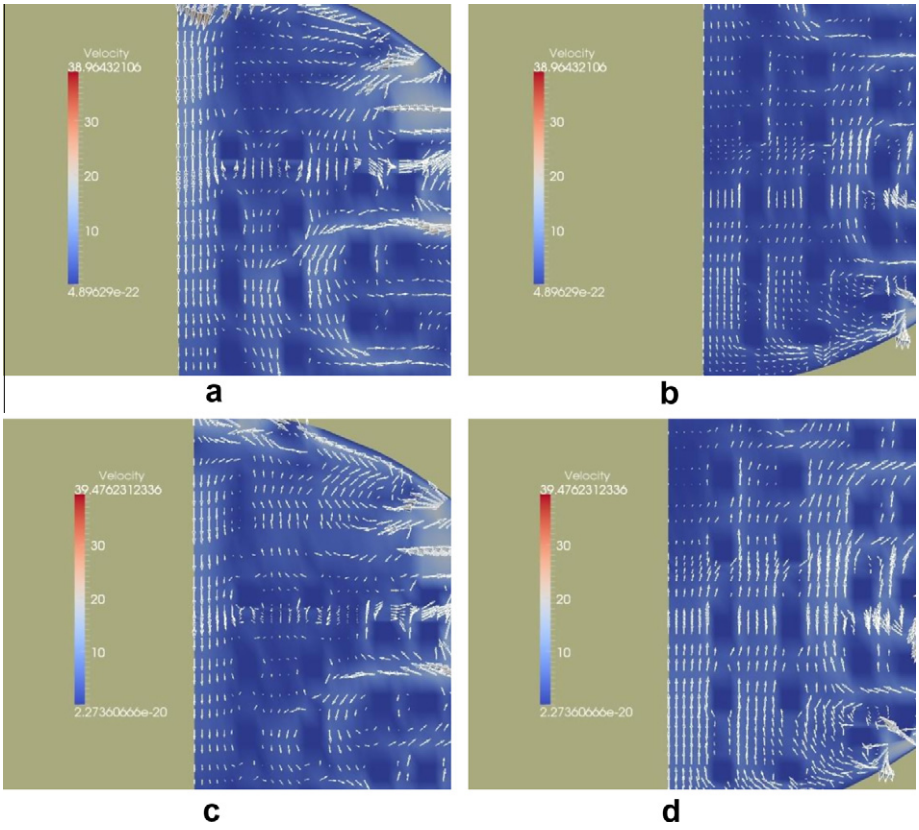

Fig. 10. Top and bottom sections of the SUPO reactor showing the time averaged liquid (a and b) and gas (c and d) phase velocity.

$\mu_{fluid} = 0.004322$ and the thermal conductivity $k_{fluid} = 0.00656$. The pipe Reynolds number is $Re_{pipe} = \frac{|v_{fluid}| d_{pipe}}{\mu_{fluid}}$. Taking into consideration the scaling for the volume fraction of the fissile solution (α_l), the heat transfer coefficient is given by:

$$h = \frac{\alpha_l Nu \; k_{fluid}}{d_{pipe}}. \tag{29}$$

In practice the heat transfer coefficient will be calculated for each element e on the fissile solution mesh. This is given as:

$$h_e = \frac{\alpha_{le}(Nu)_e \; k_{fluid}}{d_{pipe}}, \tag{30}$$

where $(Nu)_e$ denotes the average value of Nu inside element e. These values are used in the parameterisation of heat transfer at the unresolved scales for which the rate of exchange of heat is given by:

$$k_{fluid} \frac{\partial T_l}{\partial n} = h(T_w - T_l), \tag{31}$$

where n is the unit vector which is normal to the pipe and points inwards. Multiplying Eq. (26) by the control volume basis function Q_i and integrating over the pipe one obtains:

$$\int_{V_{pipe}} Q_i (V_R C_{p_{st}} \rho_{st} \frac{\partial T_{st}}{\partial t} + C_{p_w} \rho_w \frac{D_{u_w} T_w}{Dt}) dV + \int_{\Gamma_{pipe}} Q_i (hT_w - (\widehat{hT_l})) d\Gamma = 0, \tag{32}$$

where V_{pipe} is the pipe volume and Γ_{pipe} the pipe surface. By assuming the water and steel to have the same temperature, $T_{st} = T_w$, Eq. (32) is simplified to:

$$V_R C_{p_{st}} \rho_{st} \frac{\partial T_{wi}}{\partial t} + C_{p_w} \rho_w \left(\frac{D_{u_w} T_w}{Dt} \right)_i + \frac{C_{pipe\ outer}}{A_{water}} (\hat{h}_i T_{wi} - (\widehat{hT_l})_i) = 0, \tag{33}$$

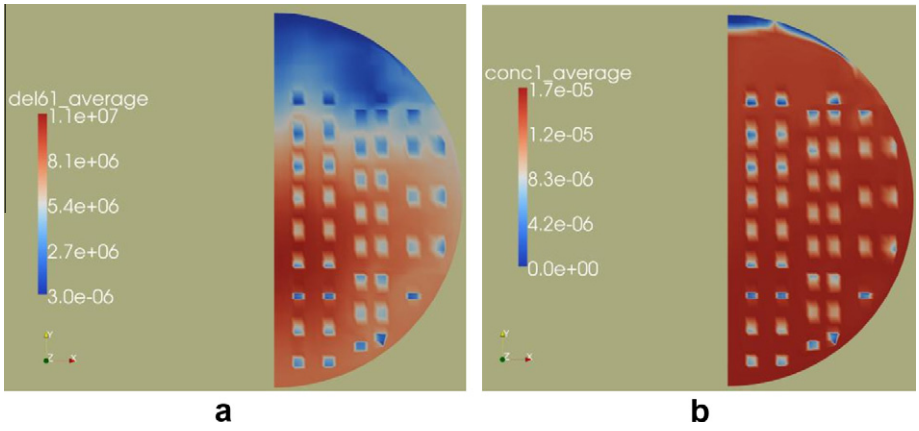

Fig. 11. (a) Time-averaged shortest-lived delayed neutron precursor concentration and (b) dissolved radiolytic gas concentration (g cm^{-3}).

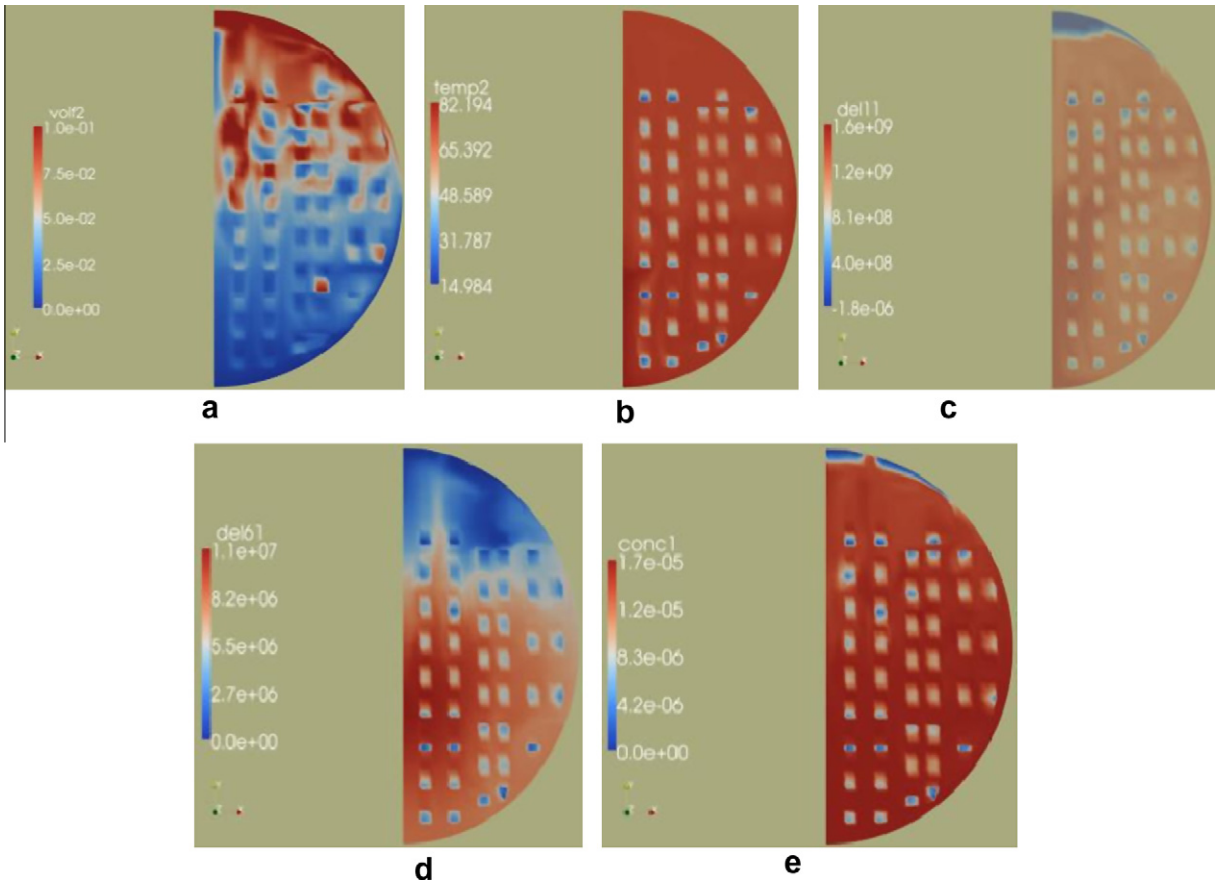

Fig. 12. These pictures show snap shots of SUPO at time instance 2264 s into the transient simulation. (a) Gas volume fraction, (b) temperature, (c) longest delayed neutron precursor, (d) shortest lived delayed neutron precursor (e) concentration of dissolved gas.

where $C_{pipe\ outer}$, A_{water} and A_{outer} denote the pipe's outer circumference, cross sectional area occupied by the water and total cross section area. The top hat marks the heat transfer variables that are mapped from the FETCH model and these will be described in the next subsection. $V_R = \frac{A_{outer} - A_{water}}{A_{water}}$. By comparing Eq. (33) with Eq. (26) the absorption σ_w and the source S_w values on pipe at control volume i can now be estimated as:

$$\sigma_{wi} = \frac{C_{pipe\ outer}}{A_{water}} \hat{h}_i, \tag{34}$$

and

$$S_{wi} = \frac{C_{pipe\ outer}}{A_{water}} (\widehat{hT_l})_i. \tag{35}$$

4.3. Heat exchanges between the pipe sub-model and the RZ FETCH SUPO model

In order to transfer information between a cooling coil and the RZ FETCH model, a set of basis functions $G_k(s)$, $k \in \{1,2,\ldots,N_{coil}\}$, are defined where N_{coil} denotes the number of intersections, or turns, that the coil makes with the RZ plane. The variable s denotes

the arc length along the pipe and so varies from $s_{in} = 0$ at the pipe's inlet to s_{out} at its outlet. Each function $G_k(s)$ is associated with the kth intersection point and centres over a node positioned at s_k which is the distance along the pipe where the kth intersection occurs. These functions are similar to standard 1D finite elements in that they have the value 1 over their respective node and fall away linearly to the value zero on their neighbouring nodes. Beyond their neighbouring nodes, the functions have zero value.

In transferring heat between the models the following lumped variables are defined:

$$L_k = \int_{coil} G_k \, ds, \tag{36}$$

which essentially provides a measure of the length of pipe about intersection k, and

$$\overline{T}_{wk} = \frac{\int_{coil} G_k T_w \, ds}{\int_{coil} G_k \, ds}, \tag{37}$$

which is the coil's water temperature, weighted with the basis functions G_k, and integrated across the length of the coil. This provides an average temperature of the pipe's water about intersection k. In addition, the heat transfer coefficient expressed at the centre of the coil's control volume M_i (this is at point point s say) is given by:

$$\hat{h}(s) = \sum_{k=1}^{Ncoil} G_k(s) \bar{h}_k. \tag{38}$$

This expression is used to define the absorption term of Eq. (34). Its value is dependent on the average heat transfer coefficient from the fluid mesh, and this is calculated through a volume average of the heat transfer coefficient about the region of intersection k (in the RZ model). That is, at each intersection k the heat transfer coefficient is calculated as:

$$\bar{h}_k = \frac{\sum_{e \in \mathcal{E}_k} \int_V M_e h_e \, dV}{\sum_{e \in \mathcal{E}_k} \int_V M_e \, dV}, \tag{39}$$

where the summation runs over the elements of the fluids mesh that contain fissile solution and that are adjacent to the pipe's kth intersection (this set is denoted by $\mathcal{E}_k$). A similar expression is used to generate an average heat exchange term centred about the kth coil intersection:

$$(\overline{hT_l})_k = \frac{\sum_{e \in \mathcal{E}_k} \int_V M_e h_e T_{le} \, dV}{\sum_{e \in \mathcal{E}_k} \int_V M_e \, dV}, \tag{40}$$

which can then be used to represent the heat exchange that takes place on the 1D pipe sub-model over control volume i:

$$(\widehat{hT_l})_i = \sum_{k=1}^{Ncoil} G_k(s_i) (\overline{hT_l})_k. \tag{41}$$

This term provides the required expression for the source term in Eq. (35) to be calculated.

It now remains to calculate the absorption term of the heat equation in the RZ SUPO model that accounts for the heat lost to the cooling coils. The approach is to take the temperature Eq. (23) for the fissile liquid and to multiply it by a control volume basis function M_e, and integrate this over the domain V. This gives the following expression:

$$\int_V M_e C_{p_l} \alpha_l \rho_l \left(\frac{D_{u_l} T_l}{Dt} \right)_e dV + \int_{\Gamma_{pipe}} M_e^S h (T_l - \overline{T}_{wK(e)}) d\Gamma = \int_V M_e S_{Tl} \, dV, \tag{42}$$

where $(.)_e$ expresses the value of the variable at the centre of element e and $\overline{T}_{wK(e)}$ is the average pipe temperature about an intersection $K(e)$ – see Eq. (37). The term M_e^S is given by:

$$\int_{\Gamma_{pipe}} M_e^S d\Gamma = \frac{\int_V M_e \, dV}{W_e} C_{pipe\ outer} L_{K(e)}, \tag{43}$$

where $W_e = \sum_{m \in \mathcal{E}_{K(e)}} \int M_m \, dV$. The index set $K(e) = k$ denotes the pipe intersection k that is adjacent to the fluid element e. The summation in W_e is therefore a volume sum of all the fluid elements that surround the intersection k. This is used to divide the volume of fluid element e ($\int_V M_e \, dV$) to give its relative volume fraction of all the elements that surround the intersection. This fraction is then multiplied by the total surface area of the pipe that surrounds the intersection k ($C_{pipe\ \text{outer}}\ L_{K(e)}$) so that M_e^S gives an expression of the surface area of the pipe in contact with element e.

Eq. (42) is now divided by the volume of the element e to give:

$$C_{p_{le}} \alpha_{le} \rho_{le} \left(\frac{D_{u_l} T_l}{Dt} \right)_e + \frac{h_e (T_{le} - \overline{T}_{wK(e)})}{\int_V M_e \, dV} \int_{\Gamma_{pipe}} M_e^S d\Gamma = S_{Tle}. \tag{44}$$

By comparing the terms in Eqs. (44) and (23), the temperature absorption terms for the fissile liquid phase can be expressed as:

$$\sigma_{le} = \frac{h_e \ C_{pipe\ outer} \int_{coil} G_{K(e)} \, ds}{W_e}, \tag{45}$$

in which h_e is the heat transfer coefficient (Eq. (29)) in element e. The temperature source for the liquid (fissile solution) phase for an element e adjacent to a pipe intersection is given by:

$$S_{le} = \sigma_{le} \overline{T}_{wK(e)} + S_{Tle}. \tag{46}$$

5. Results from the default configuration 25 kW power SUPO reactor with initial solution temperature 60 °C

The FETCH simulations presented here are based on SUPO operating at the intended 25 kW of power. The aim is not to follow a power rise to operating conditions in full detail, but to begin with initial conditions which should lead to quasi-equilibrium reasonably quickly. The simulations begin with the reactor having a solution temperature of 60 °C and a 5 °C cooling water at the pipe's inlet. The simulations are initialised with the control rod position chosen so that the reactor is in an exactly critical state. Each simulation is then allowed to evolve where by the control rod adjusts its position over time in response to the reactor's power so that it tries to maintain 25 kW of power. The heat losses from the fluid, other than through radiolytic gas release (which are small), are assumed come only from the cooling water system. There will therefore be a balance between the heat energy extracted by the cooling water and the fission power once a reactor reaches a quasi-steady-state. It should be noted that due to the nature of multiphase flow and the various feedback mechanism, this system is not expected to reach a true steady from, but instead oscillate about some average state.

In total, four simulations have been performed which vary in the speed in which their control rod can move in order to keep the reactor operating at its intended power. The first simulation used a control rod that moved with velocity 0.01 cm/s, which should only be enough to respond to long term power trends. The second simulation used a control rod velocity of 1 cm/s. Although this is considered to be quite excessive in a reality, it has been used here to demonstrate its ability to keep up with the short term power trends including those associated with transient bubble formation. In order to eliminate the effect of the control rod movement a third simulation was performed with the control rod set in a static position. In this case the rod's height was chosen so that the reactor achieved on average approximately 25 kW. Finally the fourth simulation presents a mesh-convergence test. This simulation used a rod velocity 0.01 cm/s, but the spatial discretisation was increased in resolution to that used in the first simulation. In

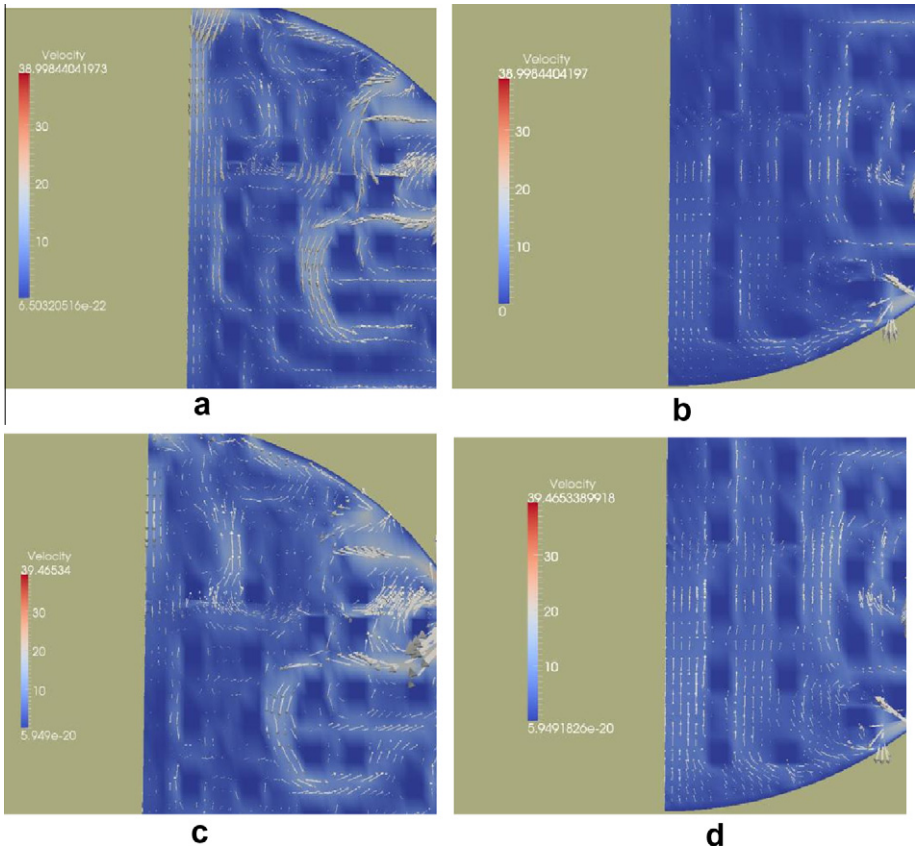

Fig. 13. Snap shots of the top and bottom sections of the SUPO reactor showing the velocity field (in cm/s) of the fissile solution (a and b) and gas phase (c and d) at 2264 s within the transients.

all calculations the SUPO reactor was simulated for 40 min of real time from its initial condition stated above.

5.1. The initial SUPO simulation

This section presents the first simulation of the SUPO reactor that was allowed to evolve over time whilst being regulated by the control rod with velocity 0.01 cm/s. The graphs presented in Fig. 6 show the real time series of SUPO's maximum power and pressure, mean outflow of cooling water temperature and heat transfer coefficient. The power shown in Fig. 6a is remarkably steady and changes by about 5% after the initial transient. This result highlights the fact that the SUPO simulation does not reach a steady state. Instead it has formed into a quasi-steady state since the power trace exhibits a noise due to the various feedback effects – eg. gas bubble production and its eventual escape through the solution surface. Fig. 6b shows the maximum pressure which again shows a steady profile once the reactor has reached its quasi-steady-state. The remaining graphs of Fig. 6 show the mean cooling water outlet temperature to be 33 °C and the mean heat transfer coefficient to be 0.14 W/cm/K. Again these two profiles are subject to noise and this would be a result of the fluctuations observed in the reactor's power. The maximum gas and fissile solution velocities and temperatures are shown in Fig. 7. This shows the maximum fissile solution temperature to only vary by a few degrees (Fig. 7d). The distance along each of the three pipes versus cooling water temperature is shown in Fig. 8. This shows a substantial variation in the cooling water temperature (≈25–30 °C) within the pipes for which the third (or outer) pipe is approximately 10% higher than the two inner coils. From this simulation it was found that once the reactor reached its quasi-steady-state, the mean fissile solution temperature was 72 °C.

It should be noted that the heat removal from the vessel, assessed on the basis of the modelled temperature rise across the coolant tubes, exceeds by about 10% that derived from the data in King (1956). However these referenced estimates take account of two additional heat loss mechanisms – heat loss to the reactors recombiner and to vessel's the graphite reflector. Together these amount to 8% of the total heat and this, in turn, will reduce the demand to transfer heat to the cooling coils. As the current FETCH model assumes all fission heat appears as a temperature rise in the solution, and that heat removal is only though the cooling coils, an increase in cooling coil temperature would be expected. The simulated results are therefore encouraging and highlight the additional heat loss to be an area for more detailed analysis. This might also explain the temperature difference between the predicted 70 °C compared with the expected 60 °C.

Figs. 9–11 present the 'time averaged' profiles of reactor's field variables associated with both the neutronic and fluid dynamics. By time average it is meant that the average of each field variable is taken over the final 30 min of the simulation – the time period where the reactor was operating in its quasi-steady-state. The time-averaged gas volume fraction and temperatures are presented (Fig. 9) and show a gradual increase in gas volume fractions with height. There are also low and high gas volume fractions on above and below the cooling coils, respectively, and this shows the gas becoming trapped and accumulating under them. The temperature of the solution outside the cooling coils varies only marginally by a few degrees.

The time averaged fissile liquid and gas velocities are shown in Fig. 10. It can be seen clearly that there are two distinct regions of

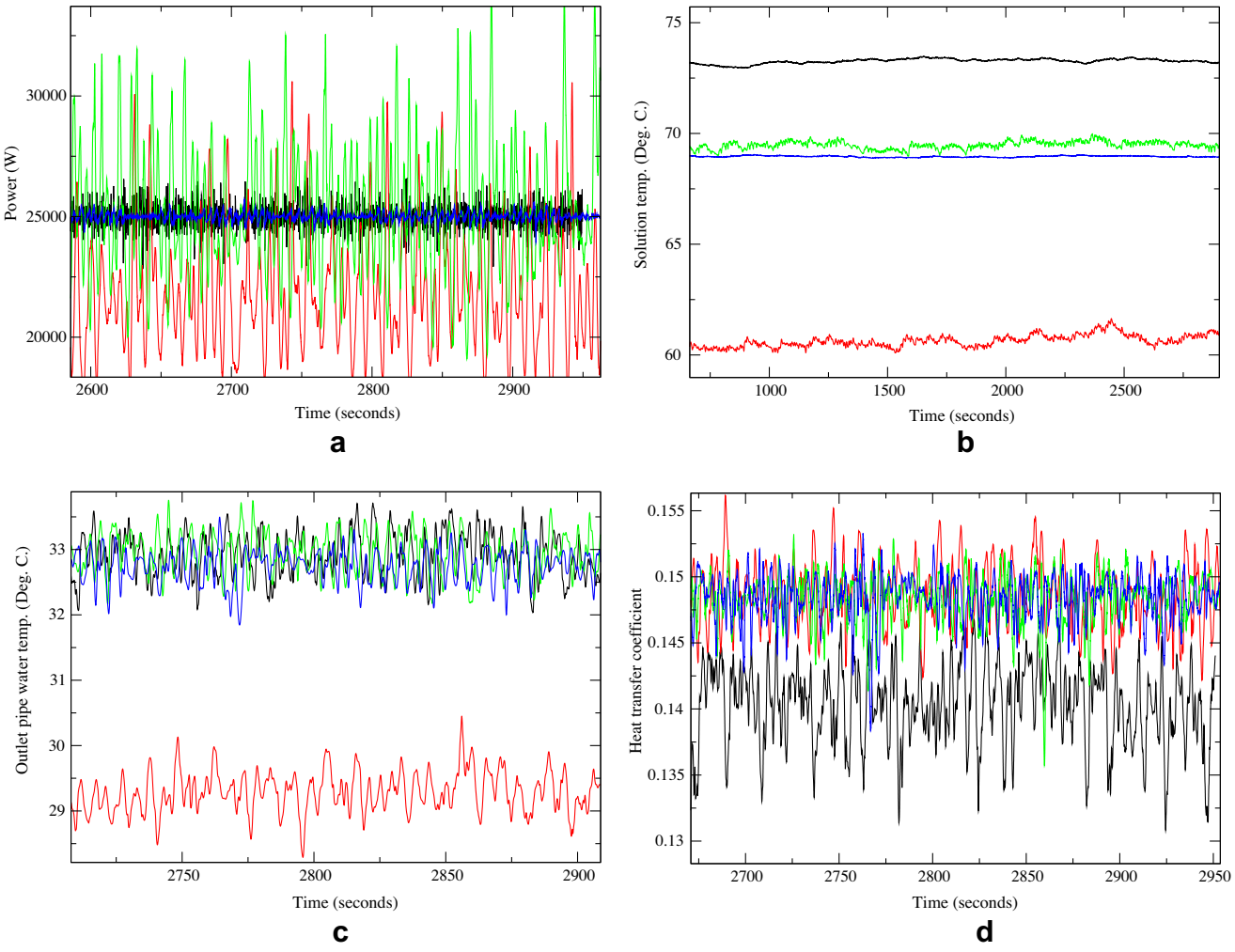

Fig. 14. Time series of several fields: (a) power (in W), (b) average solution temperature (in °C) (c) mean outlet cooling water temperature (in °C) and (d) mean heat transfer coefficient in the cooling water – fissile solution system (in W cm^{-1} K^{-1}). Black is the fine mesh standard case. Red the simulation result with a fixed control rod. Green is with slow control rod movement and blue with fast control rod movement. (For interpretation of the references to colour in this figure legend, the reader is referred to the web version of this article.)

flow. In the top region of the reactor the liquid moves down in the central region and up at the sides. In the lower region the liquid rises in the vessel's centre (due to buoyancy forces generated by radiolytic gas bubbles) and falls near the walls. This results in two distinct regions of isolated flow. The shortest-lived delayed neutron precursor concentration is shown in Fig. 11a, which illustrates the power distribution of SUPO. The power is relatively low in the upper region and this is due to the presence of the control rod. The time-averaged concentration of dissolved radiolytic gases (see Fig. 11b) is fairly uniform through the solution and is approximately equal to the critical concentration (given by Henry's law) of radiolytic gases dissolved in the solution at which bubbles start to form.

A snap shot of SUPO taken 2264 s into the simulation is presented in Fig. 12. At this time instance the quasi-steady-state conditions has been attained and Fig. 12a shows the gas volume fraction to be highly non-uniform. However the temperature is still fairly uniform as shown in Fig. 12b. Non-uniformity is also seen in the longest-lived delayed neutron concentration field that is shown in Fig. 12c. However, the shortest-lived delayed concentration (or power distribution) in Fig. 12d looks similar to the time-averaged fields shown in Fig. 11a. Also, the concentration of dissolved gas is still fairly uniform and near the critical concentration, this is shown in Fig. 12e. The instantaneous velocities shown in Fig. 13 still show the two circulation regions mentioned in the time average distributions.

5.2. Analysis of the transient simulation with variation in the spatial discretisation and control rod speed

The numerical simulations of the four test-cases with varying control rod speed and spatial meshes are compared. Fig. 14 shows the time-series of several of the reactor's fields including: power, mean solution temperature, mean outflow cooling water temperature and mean heat transfer coefficient. The power versus time plot, Fig. 14a, shows that the variation in fission rate is minimal with the fastest control rod and varies by approximately 15% for the static control rod. Again this shows that the reactor enters a quasi-steady-state for all simulations. They all oscillate about some mean state with the noise, due to the feed back effects, being dampened with a faster responding control rod. Average solution temperature for all cases (Fig. 14b), has a small variation of 0.2 °C and the mean outlet cooling water temperature versus time (Fig. 14c) varies by 1 °C for all cases. The mean heat transfer coefficient (averaged along all the pipes) (Fig. 14d), changes by approximately 5% over the course of the simulation.

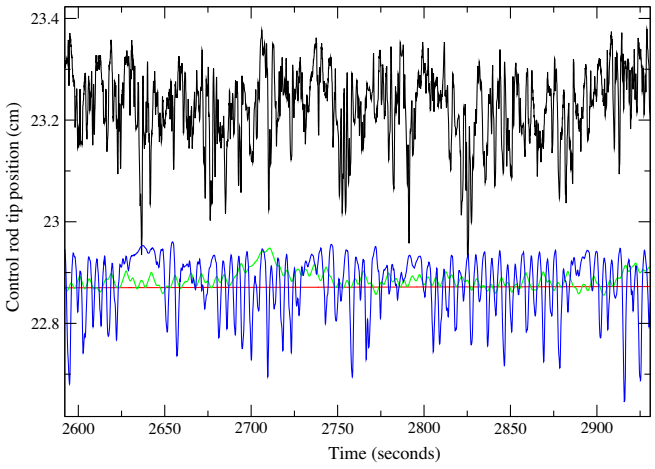

Fig. 15. Time series of control rod tip position verses time (in cm from the vessel's base). Black indicates the fast moving rod on the fine mesh, red indicates the fixed rod on the standard mesh, green the slow moving rod on the standard mesh and blue the fast rod on the standard mesh. (For interpretation of the references to colour in this figure legend, the reader is referred to the web version of this article.)

The time-series of control rod tip's position (from the vessel's base) versus time is shown in Fig. 15. These show the control rods continually moving in and out of the vessel which will be in response to the noisy power profile. The simulation with rapid 1 cm/s rod movement shows a large variations in the tip position while the slow movement case (0.01 cm/s) shows little variation as the response is effectively time averaged. Finally, using the finer spatial mesh serves to decrease the simulated reactivity slightly, and this results in a higher control rod tip position but with a similar variation about its mean.

6. Conclusion

The Modelling of the time dependent, coupled neutronic and fluid dynamics of the SUPO reactor has been conducted using the FETCH model. The simulation has modelled the reactor in RZ geometry which resolves the fuel solution in terms of multi-phase flow (consisting of both liquid and gas) in conjunction with the neutronics, together will their feedback effects. The models are run with a semi-explicit representation of the cooling coils and a 'sub model' method, which has been developed here, is then used to transfer heat from the bulk fluid into the coil's water. An adaptive control rod movement algorithm with varying velocity is also used in the simulation. Using this algorithm the rod's insertion length is constantly adjusted to respond to changes in reactivity with the aim to keep the reactor operating at 25 kW. Overall, FETCH is an excellent tool to analyse dynamics of SUPO. This investigation has not only shed some light on its dynamics that were not previously recorded during its operation (such as flow patterns and long term power trends), but also the simulation agreed well with data that was recored, such as its heat transfer. The conclusions of this study are:

(a) When modelling the 25 kW condition data set using the adaptive control rod algorithm to achieve quasi-steady power conditions, it has been assumed in the FETCH model that all fission heat arising in the solution is removed by the three cooling coils. The predictions of the modelled coolant outlet temperatures and those measured in SUPO itself are encouragingly close when the estimated 6% heat loss by conduction to the surrounding graphite reflector is taken into consideration. This loss will be accounted for in future modelling so that any residual differences in solution temperature may be ascribed to errors in solution-to-coils heat transfer algorithms (taken together with any effects of moving from 2D to 3D FETCH modelling). We consider that both heat losses through conduction and losses due to escape of the 'mobile' part of the fission energy release residing in fast neutrons and gamma rays (bearing in mind the very small SUPO core) should be assessed.

(b) Using two different averaging times, modelled high resolution traces of control rod movement in maintaining a quasi-steady power have been obtained. The observed fine scale time structure is due to the reactivity feedback effects of bubble formation, movement etc and also its effect on free surface levels. This fine scale trace could be analysed to yield further information on the stability of SUPO at its normal operating power – or at higher powers which were utilised earlier in the reactor life and when suggestions were made regarding localised boiling between coils.

(c) There are two basic flow recirculation zones that form in the 2D simulations. It is not clear if this would be the case with 3D modelling of SUPO. SUPO modelling shows a relatively homogeneous temperature distribution with the temperature varying only a few degrees across the reactor. There is a gradual increase in time-averaged gas volume fraction as we move up through the solution. Remarkably, this average is (with the exception of around the cooling coils) approximately uniform in the horizontal.

(d) We notice in the modelling a fairly dense liquid with few bubbles immediately above individual cooling coils – with a relatively large liquid volume fraction, in a time averaged sense, below the tube. Below a tube there is a concentration of trapped gas whereas above it there is a relatively low concentration of radiolytic gases due to the gas bubbles leaving this area and not being replace from below.

Acknowledgements

We are grateful for the support provided by Babcock & Wilcox and Imperial College HPC. Andrew Buchan would like to acknowledge the support of the MBASE Grant funded by the EPSRC ref: EP/I002855. Dr. M.D. Eaton would like to acknowledge the support of The Royal Academy of Engineering and EPSRC under their Research Fellowship Scheme. Mr. C.M. Cooling would like to acknowledge the support of EPSRC under their industrial doctorate programme as well as industrial support from B&W TSG.

References

Barbry, F., Fouillaud, P., 1996. Review of study programmes on criticality accidents. In: Workshop on Criticality Accident analysis ANS/ENS International Meeting.

Beck, C., Menius, A., Murray, R., Underwood, N., Waltner, A., Webb, G., 1952. Further Design Features of the Nuclear Reactor at the North Carolina State College. Technical Report AECU-1986. North Carolina State College.

Bunker, M., 1963. Status Report on the Water Boiler Reactor. Technical Report LA-2854. Los Alamos Scientific Laboratory.

Bunker, M., 1983. Early Reactors: From Fermi's Water Boiler to Novel Power Prototypes. Los Alamos Science.

de Oliveira, C.R.E., 1986. An arbitrary geometry finite element method for multigroup neutron transport with anisotropic scattering. Prog. Nucl. Energy 18, 227.

Dunenfeld, M., 1962. Kinetic Experiments on Water Boilers. 'a' Core Report, Part II, Analysis of Results. Technical Report NAA-SR-5416. Atomics International Div. of North American Aviation, Inc.

Durham, F., 1955. Radiolytic-gas bubbling improves convective heat transfer in SUPO. Nucleonics 13, 42–46.

Flora, J., Gardner, E., Greenfield, M., Roecker, J., Stitt, R., 1962. Kinetic Experiments on Water Boilers, 'a' Core Report Part I, Program History, Facility Description and Experimental Results. Technical Report NAA-SR-5415. Atomics International Div. of North American Aviation, Inc.

Gamble, D., 1959. A proposed model of bubble growth during fast transients in the KEWB reactor. Nuclear Science and Engineering 2, 213–214 (Atomics International Report NAA-SR-MEMO 3320).
IAEA, 2008. Homogeneous Aqueous Solution Nuclear Reactors for the Production of mo-99 and Other Short-lived Radioisotopes. Technical Report IAEA-TECDOC-1601. International Atomic Energy Agency.
Kasten, P., 1954. Reactor dynamics of the Los Alamos water boiler. Chem. Eng. Prog. Sympos. Ser. 11, 229–244.
King, D., 1952. The Los Alamos Homogeneous Reactor, SUPO Model. Technical Report LA-1301. Los Alamos Scientific Laboratory.
King, L., 1956. Design and description of water boiler reactors. In: Nations, U. (Ed.), Proc. International Conference on the Peaceful Uses of Atomic Energy, vol. 2, Geneva, Switzerland, p. 372391.
King, L., 1990. The Los Alamos water boiler program 1943–1974. Am. Nucl. Soc..
Lane, J., McPherson, H., Maslan, F., 1958. Fluid Fuel Reactors. Addison-Wesley Publishing Co..
Los Alamos Scientific Laboratory, 1951. An enriched homogeneous nuclear reactor. The Review of Scientific Instruments 22(7), 489–499.
Lyon, R., 1953. Preliminary Report on the 1953 Los Alamos Boiling Water Experiments. Technical Report CF-53-11-21. Oak Ridge National Laboratory.
Mather, D., Buckley, A., Prescott, A., 1994. Critex – A Code to Calculate the Fission Release Arising from Transient Criticality in Fissile Solutions. Technical Report CS/R1007/R. AEA.
Mather, J., Barbry, A.M., 1991. Examination of some fissile solution scenarios using critex. In: Proc. of the Fourth Int. Conf. Nuc. Crit. Safety.
Mather, J., Bickley, A., Prescott, A., Barbry, F., Fouillaud, P., Rozain, J., 1996. Validation of the critex code. In: Proc. of the Fourth Int. Conf. Nuc. Crit. Safety.
Nelson, C., Mann, M., 1955. Study of Incident Involving Fuel Leak in North Carolina State College Reactor. Technical Report. North Carolina State College, Collection College of Engineering Dean's Office.
Newton, T.D., Hutton, J.L., 2002. The next generation wims lattice code: Wims9. In: PHYSOR 2002, Seoul, Korea.
North American Aviation, I., 1954. Nuclear Reactor for Medical Research. Technical Report NAA-AER-1023. North American Aviation, Inc.
Pain, C.C., de Oliveira, C.R.E., Goddard, A.J.H., Umpleby, A.P., 2001a. Non-linear space-dependent kinetics for the criticality assessment of fissile solutions. Prog. Nucl. Energy 39 (1), 53–114.
Pain, C.C., de Oliveira, C.R.E., Goddard, A.J.H., Umpleby, A.P., 2001b. Transient criticality in fissile solutions – compressibility effects. Nucl. Sci. Eng. 138, 78–95.
Rosenthal, M., 2003. Nuclear Reactors Built, Being Built and Planned in the United States. Technical Report DOE/NE-0118. DOE.
Schulberg, M., 1965. Nuclear Safety Accident Analysis, Chapter The KEWB Program, pp. 386–402.
Shorthall, J., Flora, J., Graham, R., Strain, E., 1954. Power Calibration of the Water Boiler Nuclear Reactor. Technical Report LRL-149. Livermore Research Laboratory.
Soo, S., 1990. Multiphase Fluid Dynamics. Science Press.
Spiegler, P., Jr, C.B., Norman, A., 1962. Production of Void and Pressure by Fission Track Nucleation during Power Bursts in a Solution Reactor. Technical Report NAA-SR-7086. Atomics International Div. of North American Aviation, Inc.
Stitt, R., 1959. A summary of experimental results of the spherical core investigations in the KEWB program. Nucl. Sci. Eng. 2, 212–213.
Thomas, D., 1953. Preliminary Boiling Experiments in the SUPO Model of the Water Boiler. Technical Report CF-53-7-221. Oak Ridge National Laboratory.